The Plant Cell, Vol. 25: 3022–3038, August 2013, www.plantcell.org

Identification of Myosin XI Receptors in *Arabidopsis* Defines a Distinct Class of Transport Vesicles[W][OPEN]

Valera V. Peremyslov,[a] Eva A. Morgun,[a,b] Elizabeth G. Kurth,[a] Kira S. Makarova,[c] Eugene V. Koonin,[c] and Valerian V. Dolja[a,1]

[a] Department of Botany and Plant Pathology and Center for Genome Research and Biocomputing, Oregon State University, Corvallis, Oregon 97331

[b] Department of Cell Biology and Molecular Genetics, University of Maryland, College Park, Maryland 20742

[c] National Center for Biotechnology Information, National Library of Medicine, National Institutes of Health, Bethesda, Maryland 20894

To characterize the mechanism through which myosin XI-K attaches to its principal endomembrane cargo, a yeast two-hybrid library of *Arabidopsis thaliana* cDNAs was screened using the myosin cargo binding domain as bait. This screen identified two previously uncharacterized transmembrane proteins (hereinafter myosin binding proteins or MyoB1/2) that share a myosin binding, conserved domain of unknown function 593 (DUF593). Additional screens revealed that MyoB1/2 also bind myosin XI-1, whereas myosin XI-I interacts with the distantly related MyoB7. The in vivo interactions of MyoB1/2 with myosin XI-K were confirmed by immunoprecipitation and colocalization analyses. In epidermal cells, the yellow fluorescent protein–tagged MyoB1/2 localize to vesicles that traffic in a myosin XI–dependent manner. Similar to myosin XI-K, MyoB1/2 accumulate in the tip-growing domain of elongating root hairs. Gene knockout analysis demonstrated that functional cooperation between myosin XI-K and MyoB proteins is required for proper plant development. Unexpectedly, the MyoB1-containing vesicles did not correspond to brefeldin A–sensitive Golgi and post-Golgi or prevacuolar compartments and did not colocalize with known exocytic or endosomal compartments. Phylogenomic analysis suggests that DUF593 emerged in primitive land plants and founded a multigene family that is conserved in all flowering plants. Collectively, these findings indicate that MyoB are membrane-anchored myosin receptors that define a distinct, plant-specific transport vesicle compartment.

INTRODUCTION

Due to their large size, eukaryotic cells require a transport network that orchestrates the movement of endomembranes and other macromolecular complexes through the viscous cytosolic maze and delivers them to their subcellular destinations. This network relies on ATP- or GTP-hydrolyzing molecular motors that sustain traffic along either microtubules (kinesins and dyneins) or actin microfilaments (myosins) (Vale, 2003). Generally, animal cells are believed to rely on microtubule-associated motors for long-distance cargo transport, whereas actomyosin-dependent transport is used primarily for the short-distance cargo delivery and anchoring (Woolner and Bement, 2009). This concept has been recently challenged in a study that implicates actomyosin in long-range carrier vesicle transport in mouse oocytes (Schuh, 2011). In contrast with animal cells, fungal and plant cells are thought to be actin centric (i.e., they appear to rely on myosins for most of the cargo trafficking, including that of carrier vesicles and other endomembranes) (Shimmen and Yokota, 2004; Smith and Oppenheimer, 2005; Szymanski and Cosgrove, 2009; Hammer and Sellers, 2012; Brandizzi and Wasteneys, 2013).

Because of the vital roles of the carrier vesicle transport in cell growth and function, the mechanisms of vesicle formation and fusion with the target membranes have been extensively studied (Bonifacino and Glick, 2004; Südhof and Rothman, 2009; Brandizzi and Barlowe, 2013). However, the physical transport of vesicles to their subcellular destinations is poorly understood. Our current knowledge on this transport is largely derived from the yeast model. The yeast class V myosin Myo2p is an essential motor that carries organelles and vesicles to a growing bud (Schott et al., 1999, 2002; Fagarasanu et al., 2010; Donovan and Bretscher, 2012; Hammer and Sellers, 2012). Two types of factors have been implicated in the Myo2p-vesicle interaction, namely, Rab GTPases (Rabs) Yeast Protein32p (Ypt32p) and Secretory4 (Sec4) and phosphatidylinositol 4-phosphate (PI4P) (Lipatova et al., 2008; Jin et al., 2011; Santiago-Tirado et al., 2011). The Rabs directly interact with myosin, whereas PI4P does not. Because an increase in PI4P overrides the Rab requirement for transport, it has been proposed that an unknown PI4P-dependent myosin receptor, factor X, rather than Rabs, tethers vesicles to Myo2p (Santiago-Tirado et al., 2011). The exocyst component Sec15p also interacts with Myo2p (Jin et al., 2011); however, the exocyst engages later in the process to promote vesicle tethering and myosin release at the plasma membrane (Donovan and Bretscher, 2012) and cannot play the role of factor X, a missing central piece in the eukaryotic carrier transport machine.

[1] Address correspondence to doljav@science.oregonstate.edu.
The author responsible for distribution of materials integral to the findings presented in this article in accordance with the policy described in the Instructions for Authors (www.plantcell.org) is: Valerian V. Dolja (doljav@science.oregonstate.edu).

[W] Online version contains Web-only data.

[OPEN] Articles can be viewed online without a subscription.

www.plantcell.org/cgi/doi/10.1105/tpc.113.113704

Although the role of myosins in long-range vesicle transport in vertebrates has emerged only recently (Schuh, 2011), the short-range transport of many cargoes by recycling endosomes has been shown to depend on myosin Vb, the vesicular Rab11A, and its effector Rab11-family interacting protein-2 (Wang et al., 2008; Hammer and Sellers, 2012). Furthermore, a network of interactions involving Rab11A, myosin Vb, and exocyst subunit Sec15 is implicated in epithelial polarization (Bryant et al., 2010; Roland et al., 2011). Thus, the comparison of the yeast and vertebrate models of myosin V–dependent vesicle transport reveals important common players (Rabs and Sec15) and apparently missing core myosin receptors.

Plants present an extreme case of intracellular dynamics that involves the incessant trafficking of organelles and vesicles, in a process traditionally called cytoplasmic streaming (Shimmen and Yokota, 2004). It is widely believed that the long-distance transport of endomembranes in plants is primarily actomyosin dependent, with microtubule-based motility playing important accessory roles (Brandizzi and Wasteneys, 2013). The extensive dynamics of the plant cell interior are powered by the myosins XI, the fastest processive molecular motors known to date (Tominaga et al., 2003). Together with closely related fungal and animal myosins V, plant myosins XI belong to an ancient evolutionary lineage of the eukaryotic motor proteins (Richards and Cavalier-Smith, 2005; Foth et al., 2006). The myosins V/XI possess a head domain that binds actin and hydrolyzes ATP and a tail encompassing a regulatory IQ domain, a dimerization coiled-coil domain, and a cargo binding globular tail domain (GTD) (Vale, 2003; Pashkova et al., 2006; Li and Nebenführ, 2008). Notably, plant genomes encode multiple myosin XI paralogs (13 in *Arabidopsis thaliana*) compared with only two to three myosins V in yeast and animals (Peremyslov et al., 2011).

A recent surge in plant myosin research revealed that myosin XI-K and its three highly expressed paralogs are required for trafficking of Golgi stacks, peroxisomes, and mitochondria (Avisar et al., 2008, 2009; Peremyslov et al., 2008; Prokhnevsky et al., 2008), as well as for endoplasmic reticulum (ER) flow and organization of F-actin (Peremyslov et al., 2010; Ueda et al., 2010). Inactivation of these myosins abolished cytoplasmic streaming and affected cell expansion, polarized elongation, and plant growth (Peremyslov et al., 2010; Vidali et al., 2010), suggesting important roles of myosins XI in secretory transport. It has also been shown that the main cargoes of myosin XI-K are motile membrane bodies of unknown identity (Peremyslov et al., 2012). Taken together, these data indicate that myosin XI-K is the principal driver of multiple motor-dependent trafficking processes, whereas paralogous myosins XI perform partially overlapping accessory functions.

Here, we show that in *Arabidopsis*, myosin XI-K and other myosins XI mobilize their vesicular cargoes via attachment to transmembrane proteins that harbor a myosin binding domain of unknown function 593 (DUF593). We provide evidence that these, so far elusive, core myosin receptors define a distinct class of transport vesicles that are conserved in all flowering plants. We further show that myosin–receptor interactions contribute to normal plant growth and development.

RESULTS

Direct Interactions between Myosins XI and Proteins Containing DUF593

To characterize the mechanism of myosin XI-K attachment to its principal cargo, we performed a yeast two-hybrid (Y2H) screen using the Universal *Arabidopsis* Normalized Library and myosin XI-K GTD as the bait. Diploids were selected on 3-amino-1,2,4-triazole–containing medium lacking Leu, Trp, and His. The resulting colonies were streaked on minus-Leu/Trp/His/Ade plates with X-α-Gal (for 5-Bromo-4-Chloro-3-indolyl alpha-D-galactopyranoside) to select for the metabolic gene activity and activation of the α-galactosidase reporter. Growth-competent blue clones were analyzed by PCR and sequencing. A total of 37 clones were identified by screening under these relatively stringent conditions.

Intriguingly, 14 clones contained various cDNA fragments of the same gene *AT1go88oo* encoding a previously uncharacterized, ~125-kD protein. Preliminary bioinformatic analysis identified an N-terminal transmembrane domain (TM) and a highly conserved coiled-coil domain of unknown function (DUF593). As is common for cDNA library screens, all positive clones lacked the 5′-part of the open reading frame (ORF) encoding TM, thus allowing for nuclear import that is required for the Y2H screen. Among the remaining clones, eight corresponded to two genes (*At1g70750* and *At5g16720*) (Figure 1A) that were paralogs of *AT1go88oo* and encoded related TM- and DUF593-containing proteins of 86 and 77 kD, respectively. Given the high representation of the three paralogous genes in the screen and the presence of a predicted membrane-anchoring domain and the DUF593 domain that is highly conserved in plants (Holding et al., 2007) and is predicted to adopt a coiled-coil structure (a signature of diverse protein–protein interactions) (Woolfson et al., 2012), we considered these genes to be strong candidates for encoding the myosin XI-K receptor. Accordingly, the 125-, 86-, and 77-kD proteins mentioned above were dubbed myosin binding proteins or MyoB 1-3, respectively.

To validate the physical interaction between full-size MyoB and myosin XI-K, we used the pull-down assays, with *Escherichia coli*–expressed myosin XI-K GTD fused to maltose binding protein (MBP-GTD), and MyoB1 or MyoB2 that were fused to yellow fluorescent protein (MyoB1-YFP and MyoB2-YFP) and expressed transiently in *Nicotiana benthamiana*. The MBP- or GFP-fused bacterial β-glucuronidase variants (MBP-GUS and green fluorescent protein [GFP]-GUS, respectively) were used as controls for binding specificity. As shown in Figure 1B, both MyoB1-YFP and MyoB2-YFP bound MBP-GTD but not MBP-GUS, whereas, as expected, GFP-GUS bound only MBP-GUS due to the known ability of GUS to dimerize (Sang et al., 2005).

To determine whether MyoB1 interacts with full-size myosin XI-K in vivo, we coexpressed *Arabidopsis* MyoB1-YFP and myosin XI-K in *N. benthamiana* and performed coimmunoprecipitation assays using GFP-specific antibody immobilized on agarose beads. As shown in Figure 1C, myosin XI-K specifically coimmunoprecipitated with MyoB1 but not with free GFP.

Our analysis of the 22 interaction-positive clones isolated in the Y2H screen revealed 3′-terminal fragments of *MyoB1-3* of various sizes, all of which encoded the DUF593 domain, suggesting that this domain is responsible for binding the myosin XI-K GTD. To test

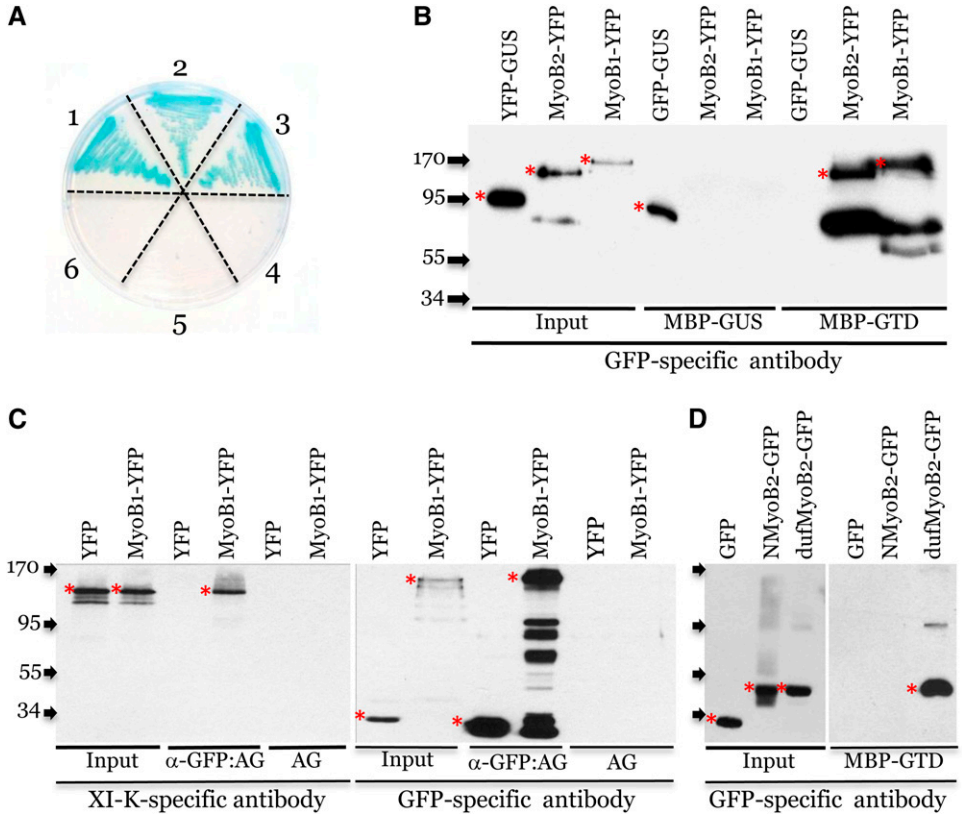

Figure 1. Interactions between Myosin XI-K and Proteins Encoded by *Arabidopsis* Genes *AT1go88oo* (*MyoB1*), *At1g70750* (*MyoB2*), and *At5g16720* (*MyoB3*).

(A) Y2H assay on SD/-Leu/-Trp/-His/-Ade plates supplemented with X-α-Gal. The combinations of bait and prey proteins used in each sector of the Petri dish were as follows: 1, XI-K-GTD + MyoB1; 2, XI-K-GTD + MyoB2; 3, XI-K-GTD + MyoB3; 4, MyoB3 + GFP; 5, MyoB2 + GFP; 6, MyoB1 + GFP.
(B) Pull-down assay showing specific binding of MyoB1-YFP and MyoB2-YFP to immobilized XI-K GTD (MBP-GTD) but not to immobilized GUS (MBP-GUS). GFP-GUS provides specificity control via binding to MBP-GUS (GUS forms dimers) but not to MBP-GTD.
(C) Coimmunoprecipitation of the MyoB1-YFP–myosin XI-K complexes formed in vivo. α-GFP:AG, GFP-specific monoclonal antibody immobilized on agarose beads; AG, uncharged agarose beads control.
(D) Pull-down assay showing specific binding of the MyoB2 DUF593 domain (dufMyoB2-GFP) to immobilized XI-K GTD (MBP-GTD). Free GFP and N-terminal fragment of MyoB2 (NMyoB2-GFP) provide binding specificity controls. Arrows at the left show protein marker positions with their molecular mass in kilodaltons. Red asterisks mark full-size protein bands; bands of lower molecular mass probably correspond to protein degradation products.

this prediction, we expressed the DUF593 domain of MyoB2 fused to GFP (dufMyoB2-GFP) and used an N-terminal fragment of MyoB2 of a similar molecular mass fused to GFP (NMyoB2-GFP) as specificity control. As shown in Figure 1D, these pull-down assays with MBP-GTD confirmed that DUF593 was sufficient for myosin binding.

To investigate the ability of MyoB to interact with other *Arabidopsis* myosins XI, we performed a Y2H screen using the *Arabidopsis* cDNA library and the GTD of myosin XI-1, a closely related myosin XI-K paralog (Peremyslov et al., 2011), as bait. This screen yielded 30 interaction-positive clones, 18 of which harbored various fragments of MyoB1 and MyoB2 cDNAs, suggesting that interaction with MyoB is a common property of plant myosins XI (see Supplemental Figure 1 online). This inference was strongly supported by an additional screen in which the bait was a GTD of myosin XI-I that is divergent from both myosin XI-K and XI-1. Strikingly, this screen also yielded a DUF593-containing protein that is encoded by *At5g06560* and is distantly related to MyoB1-3; this protein was designated MyoB7 (see phylogenetic analysis below). The pairwise Y2H assays using XI-I GTD detected interactions with MyoB1, but not MyoB2 (see Supplemental Figure 1 online).

Taken together, the results of these experiments show that distinct MyoB proteins are capable of interacting with the specific subsets of myosins XI in vitro and in vivo via direct binding between DUF593 and the myosin GTD. Because MyoB proteins also contain a predicted TM region, they are strong candidates for the core vesicular myosin XI receptors.

MyoBs Are Associated with the Myosin-Driven Cargo Membranes

To characterize the pattern of subcellular localization of MyoB1 and MyoB2, we tagged each of these proteins by fusing YFP to

their C termini. The modified genomic clones of *MYOB1* (*AT1-go88oo*) and *MYOB2* (*At1g70750*), including their native promoters, were transformed into the *Arabidopsis myob1* and *myob2* gene knockout backgrounds (see below), respectively, in order to express the MyoB1-YFP and MyoB2-YFP to levels similar to those of wild-type MyoB1 and MyoB2. Confocal laser scanning microscopy (CLSM) using plants expressing MyoB1-YFP or MyoB2-YFP revealed motile "beads-on-a-string" structures in elongated leaf epidermal cells (Figure 2A; see Supplemental Movies 1 and 2 online) that closely resembled those described for myosin XI-K:YFP (Peremyslov et al., 2012). This pattern was observed in over 90% of the imaged cells ($n \geq 20$).

Because the TM of MyoB7 is located at the C terminus of the protein, the genomic clone of *At5g06560* was modified to accommodate a YFP tag downstream of the translation initiation codon. The resulting *YFP-MYOB7* clone was transformed into *Arabidopsis*, and YFP-MyoB7 localization in the leaf epidermal cells was examined by CLSM. As shown in Figure 2A (right

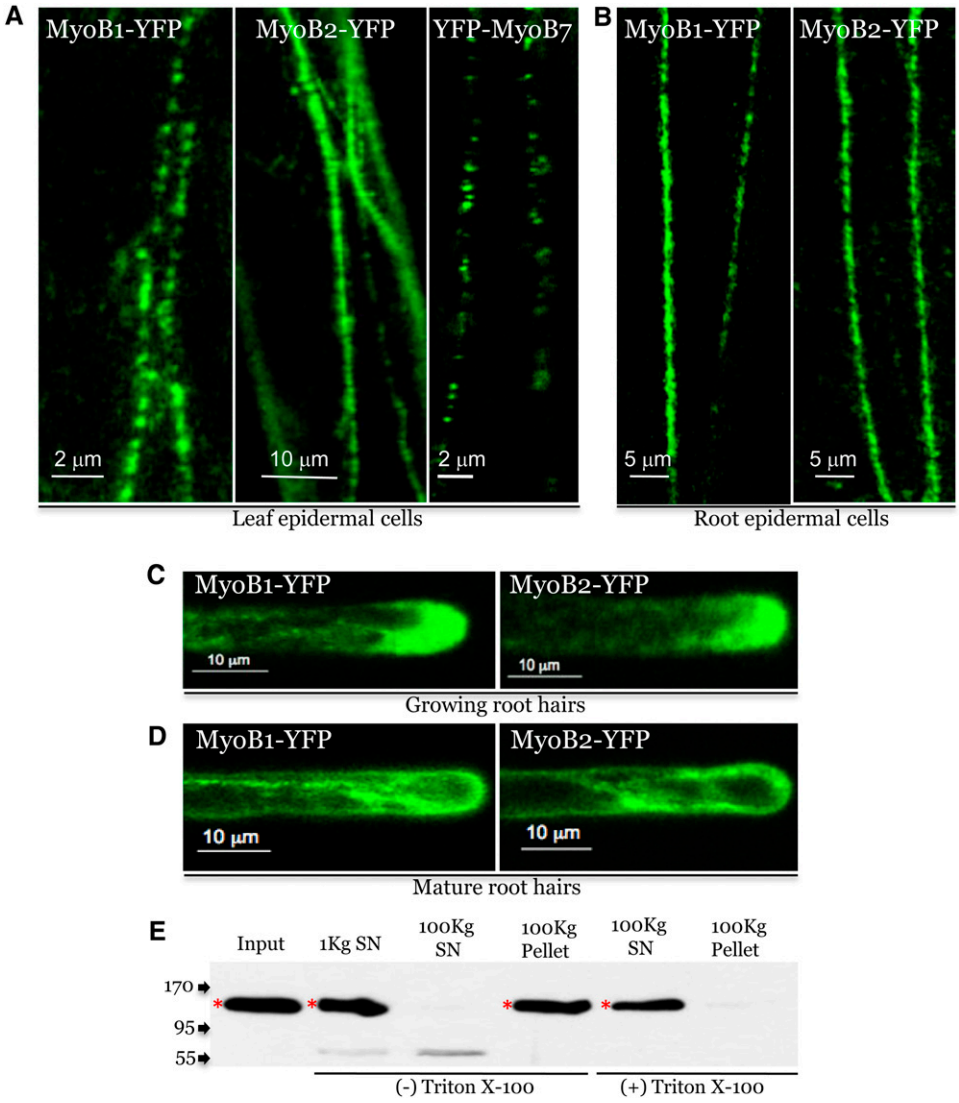

Figure 2. Subcellular Localization of MyoB1-YFP and MyoB2-YFP.

(A) Confocal images of leaf midvein epidermal cells expressing MyoB1-YFP, MyoB2-YFP, and YFP-MyoB7 in *myob1* and *myob2* genetic backgrounds, respectively.

(B) Analogous images of the root epidermal cells expressing MyoB1-YFP and MyoB2-YFP in *myob1* and *myob2* genetic backgrounds, respectively.

(C) and **(D)** Confocal images of growing **(C)** and mature **(D)** root hairs expressing MyoB1-YFP and MyoB2-YFP.

(E) Subcellular fractionation of leaf extracts from *myob1 MyoB1-YFP* plants. The 1000 g and 100,000 g supernatants (1Kg SN and 100Kg SN, respectively) and the pellets in the presence (+) or absence (−) of Triton X-100 were analyzed using immunoblotting with GFP-specific monoclonal antibody. Arrows at the left show protein marker positions with their molecular mass in kilodaltons; red asterisks mark full-size protein bands; bands of lower molecular mass probably correspond to protein degradation products.

panel) and Supplemental Movie 3 online, this reporter tagged motile bodies whose appearance was similar to those tagged by MyoB1-YFP and Myob2-YFP. Interestingly, these bodies were much more sparse compared with the denser flow of the MyoB1-YFP– or MyoB2-YFP–tagged bodies. This outcome suggested that the cargoes driven by interactions between myosins XI-K/XI-1 and MyoB1 and MyoB2 on one hand, and those driven by the interaction between myosin XI-I and MyoB7 on the other hand, might perform distinct functions.

Further analysis of the MyoB1-YFP and MyoB2-YFP distribution revealed essentially identical localization patterns in root epidermal cells (Figure 2B). Notably, both MyoB1-YFP and MyoB2-YFP concentrated in the tip-growing domains of rapidly elongating but not mature root hairs (Figures 2C and 2D), again a pattern similar to that of myosin XI-K:YFP (Peremyslov et al., 2012) and other proteins involved in polarized cell growth (Cole and Fowler, 2006). The close resemblance of the MyoB1-YFP and MyoB2-YFP localization patterns to those of myosin XI-K:YFP in distinct cell types implies that each of these candidate myosin receptors is associated with the cargoes whose trafficking is driven by this myosin.

To further validate the endomembrane nature of the round structures labeled with MyoB1-YFP, we performed subcellular fractionation and found that >95% of MyoB1-YFP was present in the 100,000*g* microsomal pellet (Figure 2E). Treatment of this pellet with Triton X-100 resulted in solubilization of MyoB1-YFP as is expected for a membrane-associated protein and in complete accordance with the results obtained for myosin XI-K (Peremyslov et al., 2012). To determine whether the targeting of MyoB to membranes depended on the predicted transmembrane region of this protein, we transgenically expressed the N-terminal portion of MyoB2 (residues 1 to 61) in *Arabidopsis* Columbia plants as a GFP fusion. The observed subcellular distribution pattern was similar to that of full-size MyoB2-YFP (see Supplemental Figure 2 online), which led us to conclude that the TM region was sufficient for the membrane targeting of MyoB1.

To determine whether the trafficking of MyoB1-YFP–tagged cargo was myosin dependent, the *MyoB1-YFP* gene was transformed into plants with three distinct genetic backgrounds: Columbia, *xi-k*, and *xi-k xi-1 xi-2*. As shown previously, the mean velocities of organelle trafficking in the *xi-k* gene knockout are reduced (Peremyslov et al., 2008), whereas in the triple myosin gene knockout, the entire intracellular endomembrane transport is nearly halted (Peremyslov et al., 2010). As seen in Figure 3A, inactivation of myosin XI-K resulted in a partial redistribution of MyoB1-YFP that was no longer limited to linear tracks, as well as in a slower motion of the marker-tagged material (see Supplemental Movie 4 online). An even more dramatic picture was observed in a triple gene knockout where MyoB1-YFP was distributed more diffusively and was essentially immotile (Figure 3A; see Supplemental Movie 5 online). We assume that in the latter case, MyoB1-YFP remained associated with the membranes although this assumption was not validated experimentally.

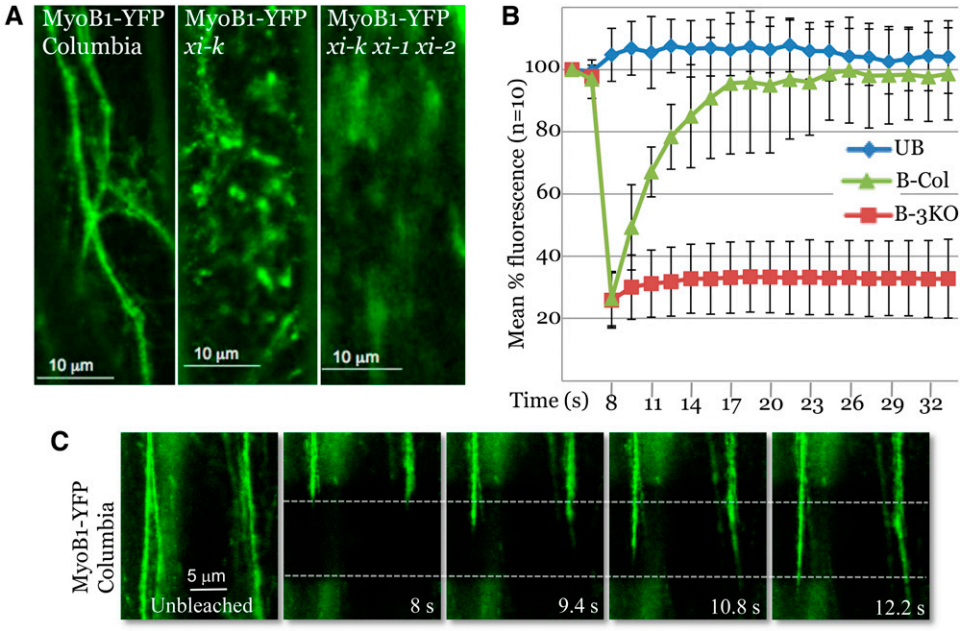

Figure 3. Confocal Imaging and FRAP Analysis of the MyoB1-YFP–Tagged Material in the Leaf Epidermal Cells of the Columbia or Myosin XI Gene Knockout Plants.

(A) The MyoB1-YFP localization patterns in the genetic backgrounds of control Columbia, *xi-k*, and *xi-k xi-1 xi-2* plants.
(B) FRAP analysis of the Columbia and *xi-k xi-1 xi-2* plants. UB, unbleached; B-Col, bleached Columbia; B-3KO, bleached *xi-k xi-1 xi-2* triple knockout.
(C) Consecutive confocal images of the Columbia MyoB1-YFP epidermal cells before (left panel) and after photobleaching. The photobleached area (dashed line) and times after treatment are shown.

Fluorescence recovery after photobleaching (FRAP) was used to further characterize and quantify the effects observed in the triple myosin knockout plants. The FRAP measurements showed nearly complete recovery of the MyoB1-YFP fluorescence in ~10 s after photobleaching in the Columbia plants (Figures 3B and 3C; see Supplemental Movie 6 online). The velocity with which the front of the fluorescent material was moving into the photobleached area (Figure 3C) was 6.32 ± 1.20 μm/s (n = 20), a value very close to the 7 μm/s velocity that has been reported for plant myosin XI in vitro (Tominaga et al., 2003). Strikingly, no statistically significant recovery of the MyoB1-YFP fluorescence was observed in *xi-k/1/2* plants over the observation period (Figure 3B; see Supplemental Movie 7 online), indicating that inactivation of the three highly expressed myosins XI (Peremyslov et al., 2011) arrested the trafficking of MyoB1-YFP–tagged cargo. Collectively, these results demonstrated that MyoB1 and MyoB2 are associated with endomembranes that presumably form vesicles and are rapidly transported in a myosin XI–dependent manner. For the sake of brevity, hereinafter we will refer to the MyoB1/2-associated membranous cargoes of myosin XI-K as "vesicles," although their size and morphology are yet to be determined by ultrastructural analysis.

In Vivo Colocalization of Myosin XI-K with MyoB1

To validate the association of MyoB1 and myosin XI-K in *Arabidopsis* cells, we used dual fluorophore real-time imaging and subcellular gradient fractionation. MyoB1-GFP and myosin XI-K:mCherry were coexpressed in the *xi-k xi-1 xi-2* triple knockout background; MyoB1-GFP rather than MyoB1-YFP was used in these experiments to ensure confident separation of the spectra of the two fluorophores. As shown previously, fluorophore-tagged myosin XI-K is fully functional and rescues the defective growth phenotype in the triple knockout plants (Peremyslov et al., 2012). Strikingly, we found that the beads-on-a-string labeled by either MyoB1-GFP or myosin XI-K:mCherry colocalized in 100% of the imaged cells (n = 44; Figure 4A).

Isopycnic Suc gradient fractionation of *Arabidopsis* leaf extracts described previously revealed comigration of myosin XI-K with some endomembrane markers, including an ER marker (Ueda et al., 2010; Peremyslov et al., 2012). We performed a similar fractionation analysis with MyoB1-YFP–expressing plants and analyzed individual fractions by immunoblotting using GFP-, myosin XI-K-, ER-, and prevacuolar compartment (PVC)–specific antibodies. The observed coincidence of the MyoB1-YFP and myosin XI-K peaks (see Supplemental Figure 3 online) was fully compatible with a physical interaction between these two proteins. As expected, these peaks closely corresponded to the ER peak but were well separated from PVC. We concluded that both the colocalization and gradient fractionation experiments corroborated an in vivo association of MyoB1 and myosin XI-K. Taken together with the myosin-dependent trafficking of the MyoB1-containing vesicles (Figure 3), these data strongly support a role of MyoB as functional membrane-anchored receptors for the myosins XI in *Arabidopsis*.

MyoB1-Decorated Transport Vesicles Comprise a Separate Endomembrane Compartment

We found previously that the myosin XI-K–decorated vesicles are transported along F-actin filaments and exhibit only limited overlap with Golgi stacks or post-Golgi vesicle clusters containing SECRETORY CARRIER MEMBRANE PROTEIN2 (SCAMP2) (Peremyslov et al., 2012). To gain further insight into the nature of these transport vesicles defined by the MyoB–myosin interactions, we employed a pharmacological approach complemented by colocalization analyses using several endomembrane compartment-specific markers.

Brefeldin A (BFA) is a potent inhibitor of secretory transport affecting the formation of COPI vesicles that is critical for the ER-Golgi interface dynamics (Brandizzi and Barlowe, 2013) and causes fusion of Golgi stacks with the ER network (Chardin and McCormick, 1999; Ritzenthaler et al., 2002; Ito et al., 2012). Accordingly, in control experiments with BFA, we observed absorption of Golgi by the ER in transgenic *Arabidopsis* plants expressing a Golgi marker alone or in combination with a spectrally distinct ER marker (Figure 4C). Furthermore, BFA treatment caused redistribution of the *trans*-Golgi network compartment marked by the small Rab GTPase YFP:RabA4b (Preuss et al., 2004; Kang et al., 2011). Instead of the relatively small vesicular bodies that were observed in untreated cells, in the BFA-treated cells, this marker localized primarily to large cistern-like bodies (Figure 4C). Surprisingly, BFA treatment had no observable effect on the vesicles tagged by MyoB1-GFP (Figure 4C). This result indicated that the MyoB1-containing vesicles do not belong to the BFA-sensitive secretory compartment.

To further decipher the relationships between exocytic and MyoB1-decorated vesicles, we coexpressed MyoB1-GFP with the exocytic vesicle marker mCherry-VAMP721, one of the plant v-SNAREs (Sanderfoot, 2007; Brandizzi and Barlowe, 2013). As shown in Figure 4B, the two markers did not colocalize; even those few mCherry-VAMP721–labeled vesicles that were present along the string of MyoB1-GFP–labeled vesicles did not coincide with the latter, but rather were located between them (arrows in Figure 4B). Thus, the MyoB1-containing vesicles do not appear to belong to a major secretory trafficking pathway.

To investigate the potential relationship between MyoB1- and myosin XI-K–decorated vesicles and endocytic pathways, we analyzed the relative localization of MyoB1-GFP and the endocytic compartments defined by clathrin and flotillin (Simons and Gerl, 2010; Chen et al., 2011; Li et al., 2012). Little spatial overlap was observed between the marker of clathrin-coated vesicles, mCherry-tagged clathrin light chain 2 (CLC2-mCherry) (Konopka et al., 2008), and MyoB1-GFP (Figure 4D). Only a few CLC2-mCherry–labeled bodies localized within the strings of the MyoB1-GFP bodies, but even these did not correspond in size and shape to the adjacent MyoB1-GFP bodies (arrows in Figure 4D). An even lesser degree of colocalization was found between MyoB1-GFP and flotillin1:mCherry (Flot1:mCherry) (Li et al., 2012), a marker of the clathrin-independent exocytic pathway (Figure 4E). Thus, there was no significant overlap between the MyoB1-GFP–decorated motile vesicles and at least two distinct endocytic compartments.

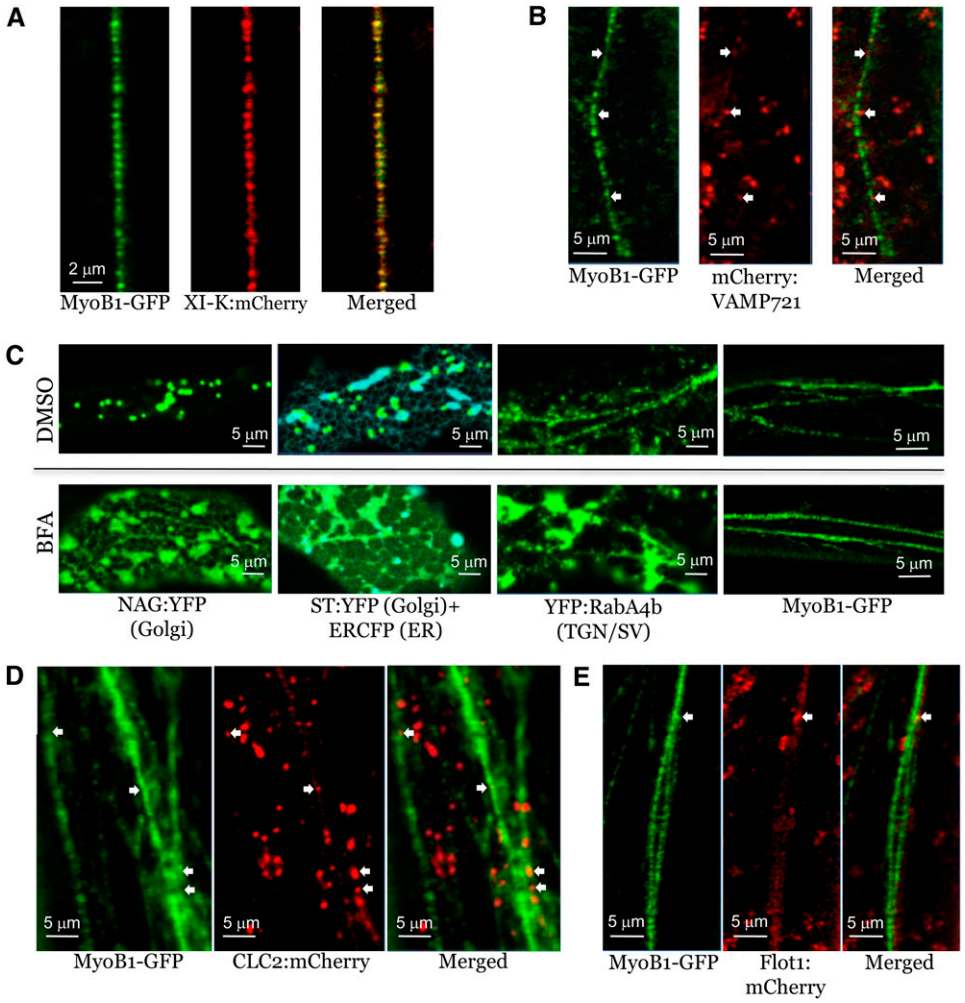

Figure 4. Analysis of MyoB1-GFP Localization Relative to Distinct Compartment-Specific Markers in the Leaf Epidermal Cells of Transgenic *Arabidopsis* Plants.

(A) Colocalization of MyoB1-GFP with myosin XI-K:mCherry in *myob1* plants.
(B) Colocalization analysis of MyoB1-GFP and exocytic vesicle marker mCherry-VAMP721 in *myob1* plants; white arrows indicate positions of a few mCherry-VAMP721–positive bodies that fall into a linear flow of the MyoB1-GFP–positive bodies.
(C) Distribution of Golgi-specific (NAG:YFP and ST:YFP), ER-specific (ERCFP), *trans*-Golgi network/secretory vesicle (TGN/SV)–specific (YFP:RabA4b) markers in Columbia plants, and MyoB1-GFP in DMSO-treated (control; top row) or BFA-treated (bottom row) leaf epidermal cells of *myob1* plants.
(D) Colocalization analysis of MyoB1-GFP and the endocytic vesicle marker CLC2:mCherry in *myob1* plants; white arrows indicate a few CLC2:mCherry-positive bodies that fall into the linear flow of the MyoB1-GFP–positive bodies.
(E) Colocalization analysis of MyoB1-GFP and the marker of non-clathrin-coated endocytic vesicles in *myob1* plants, Flot1:mCherry; white arrow denotes a Flot1:mCherry-positive body that falls into the linear flow of the MyoB1-GFP–positive bodies.

In conclusion, the presented data indicate that the motile vesicles decorated by myosin XI-K and its putative transmembrane receptor MyoB1 do not correspond to several major exocytic and endocytic compartments and most likely represent a distinct class of transport vesicles that was not described previously.

The Superfamily of DUF593-Containing Proteins Is Conserved in Land Plants

Previously, a DUF593-containing protein was identified as the product of the *Floury1* gene involved in zein protein body formation in maize (*Zea mays*) endosperm, and a large family of homologous DUF593-containing proteins was identified in rice (*Oryza sativa*) and *Arabidopsis* (Holding et al., 2007). Given the recent vast expansion in the number of sequenced plant genomes, we sought to gain a broader insight into the origin and evolution of this group of proteins. A PSI-BLAST search in the Refseq database identified 173 DUF593-containing proteins in all sequenced genomes of land plants including the nonvascular moss *Physcomitrella patens*, the vascular spikemoss *Selaginella moellendorffii*, and flowering plants, both monocots and dicots (see Supplemental Data Set 1 online). All of these plants encompass multiple, paralogous DUF593-encoding

genes. Specifically, in *Arabidopsis*, 15 genes encode a complete DUF593 domain and one gene (At2g24140) encodes an apparently incomplete one. We constructed a multiple alignment of all identified DUF593 domains (101 informative positions; see Supplemental Data Set 2 online) and used it to generate a maximum- likelihood phylogenetic tree. The resulting tree topology implies that, after the divergence from the common ancestor with the mosses, at least three families of DUF593-containing proteins, each represented in most monocots and dicots, evolved in the stem phase of the evolution of the flowering plants (Magnoliophyta) (i.e., antedating the last common ancestor of all extant plants in this phylum) (Figure 5A). The monophyly of each of these three families is supported either by a very high bootstrap value (92 and 86% for families I and II, respectively) or by a moderate bootstrap value (55% for family III) and was also reproduced using the FastTree method of phylogenetic tree construction (see Supplemental Figure 4 online).

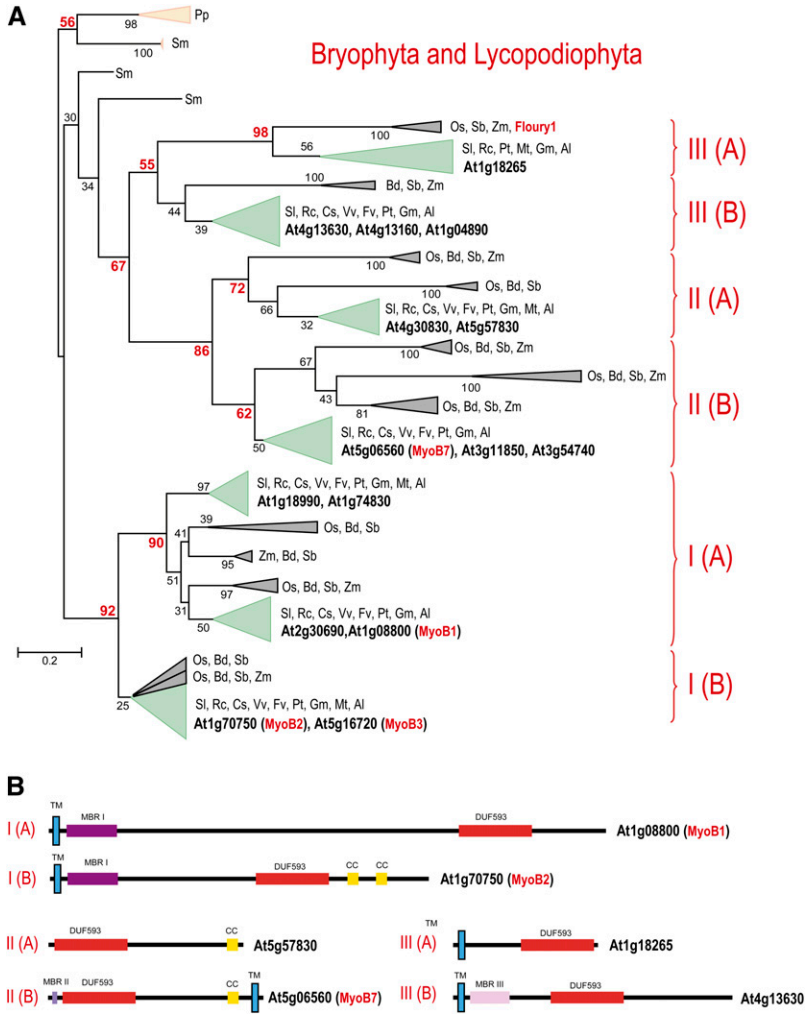

Figure 5. Phylogenetic Tree and Domain Architectures of DUF593-Containing Proteins.

(A) The unrooted maximum likelihood tree was built using the Randomized A(x)ccelerated Maximum Likelihood (RAxML) program on the basis of the multiple alignment of DUF593 domains. RAxML was also used to compute bootstrap values, which are shown for selected branches. Reliable bootstrap values supporting families and subfamilies are highlighted in red. The collapsed branches are shown by triangles according to the respective plant taxa as follows: moss and spikemoss in light brown, monocots in gray, and dicots in green. For *Arabidopsis*, the gene identifiers are highlighted by bold type. The MyoB1-3 described in this work and the previously described Floury1 (Holding et al., 2007) are shown in red. Other organisms are identified using a two-letter code as follows: Pp, *Physcomitrella patens*, Sm, *Selaginella moellendorffii*; Mt, *Medicago truncatula*; Pt, *Populus trichocarpa*; Vv, *Vitis vinifera*; Bd, *Brachypodium distachyon*; Os, *Oryza sativa*; Zm, *Zea mays*; Sb, *Sorghum bicolor*; Gm, *Glycine max*; Cs, *Cucumis sativus*; Rc, *Ricinus communis*; Al, *Arabidopsis lyrata*; Fv, *Fragaria vesca*; and Sl, *Solanum lycopersicum*. The complete tree is provided in Supplemental Figure 4 online. The bar shows the number of substitutions per site.

(B) The domain architectures of the DUF593 superfamily proteins are shown for typical representatives of each subfamily. The lengths of the proteins and domains, shown as boxes, are roughly to scale. CC, coiled-coil domain; MBRI, MBRII, MBRIII, Metal Binding Region I, II and III; TM, transmembrane domain.

Moreover, each family further split into at least two subfamilies (albeit some weakly supported by bootstrap values) that are present in the major groups of both dicots and monocots and probably are ancestral as well (Figure 5A).

We further analyzed the sequences of the DUF593-containing proteins to identify additional domains, transmembrane helices, and coiled-coil regions. These proteins show notable variability of domain architectures but also share common structural features, at least at the level of the six subfamilies (see Supplemental Data Set 1 online). The DUF593 itself is confidently predicted to adopt a coiled-coil structure, thus representing a rare case of a coiled-coil domain that maintains a strong identity over hundreds of millions years of evolution, rather than showing generic similarity to numerous other structures of this type (Aravind et al., 2006). In addition, many proteins in the DUF593 superfamily contain other strongly predicted coiled-coil regions, typically near the C terminus (Figure 5B). The majority of the proteins in this superfamily also contain a single, strongly predicted transmembrane helix that in most cases is located near the N terminus (e.g., in MyoB1-3) but in a minority of the proteins resides near the C terminus (e.g., in MyoB7; see Supplemental Data Set 1 online). The confident prediction of transmembrane helices but not signal peptides in the majority of the DUF593 superfamily proteins is compatible with their localization in intracellular membranes distinct from the ER membranes. Finally, the majority of the DUF593-containing proteins possess distinct regions with specific patterns of Cys residues (in one case, also involving a His) that are conserved within the families or subfamilies (Figure 5B). Three such patterns were detected: MBR I motif, C-x(2)-C-x(13-27)-C-x(2)-H-x(9-13)-C-x(2)-C-x(18-69)-C-x(2)-C; MBR II motif, CC-x(1-3)-C-x-C-x(1-2)-C; and MBR III motif, C-x(~47)-C-P-C-x(6-11)-C. These patterns of conserved Cys residues resemble those in known metal binding domains, such as zinc–fingers, and could be implicated in the chelation of transitional cations, such as Zn^{2+} (hence, the designation MBR, after metal binding region). However, the MBR regions in the DUF593 proteins are predicted to adopt α-helical structures and so are unrelated to Zn-fingers that form β-hairpins (Matthews and Sunde, 2002). If the prediction of metal binding is experimentally validated, the MBRs will comprise a distinct class of metal binding protein modules.

Thus, MyoB1-3, MyoB7, and Floury1 belong to the families I, II, and III, respectively, of the large superfamily of DUF593-containing proteins that apparently emerged in land plants. Given the high level of DUF593 sequence conservation (see Supplemental Data Set 2 online), it seems likely that the myosin binding described here is a common property of this domain, whereas the ability of Floury1 to bind maize-specific zeins is a specific feature of this ER-associated protein (Holding et al., 2007). This hypothesis is in agreement with the recently described roles of the *Opaque1*-encoded myosin XI in ER motility and maize protein body formation (Wang et al., 2012), which suggest cooperation between Floury1 and myosin in this process. Furthermore, the interaction between myosin XI-I and MyoB7, a family II member, described here provides further evidence in support of the functional partnership between myosins XI and the entire superfamily of DUF593-containing proteins.

Inactivation of MYOB1-4 Genes Affects Plant Growth and Flowering Time

Bioinformatics analysis of the DUF593 superfamily suggested both functional specialization (based on distinct domain architectures among proteins from six subfamilies) and a degree of functional redundancy (supported by the high level of similarity between some paralogs [e.g., MyoB2 and MyoB3]) among the superfamily members. To determine the functions of MyoB proteins in plant development, we focused on the family I members of which at least MyoB1-3 interact with the principal *Arabidopsis* myosin XI-K. This analysis also included *At2g30690*, a closely related paralog of MyoB1 (Figure 5A) designated MyoB4.

Analogously to myosins XI (Peremyslov et al., 2008), the analysis of the growth phenotypes of the four single gene knockout lines *myob1*, *myob2*, *myob3*, and *myob4*, as well as of the double gene knockout *myob2 myob3* (2KO), revealed no statistically significant differences with the Columbia control (Figures 6A and 6B). However, the triple knockout *myob1 myob2 myob3* (3KO) and the quadruple knockout *myob1 myob2 myob3 myob4* (4KO) plants exhibited a statistically significant height reduction compared with the Columbia control (~8 and ~15%, respectively; Figure 6A; see Supplemental Data Set 3 online). Interestingly, the 4KO but not 3KO mutant showed a modest, ~8% reduction in rosette diameter (Figure 6B; see Supplemental Data Set 3 online).

Because a physical interaction between MyoB1-3 and myosin XI-K implies that they function in the same transport pathway and might interact genetically, we characterized synthetic knockout mutants in which both myosin XI-K and subsets of MyoB proteins were inactivated. Strikingly, the *xi-k myob2 myob3*, *xi-k myob1 myob2 myob3*, and *xi-k myob1 myob2 myob3 myob4* mutants showed highly significant progressive defects in stem growth (see Supplemental Data Set 3 online): Their height was reduced by 12, 33, and 66%, respectively, relative to the corresponding controls (Figure 6A). However, no statistically significant differences in leaf rosette diameter were found in each of the three synthetic knockout mutants, indicating that cooperation between myosin XI-K and MyoB1-4 is more important for the growth of stems than it is for the growth of leaves.

Further analysis of the mutant plants revealed significant delays in the onset of flowering. As shown in Figure 6C, 2KO, 3KO, and 4KO plants, as well as the *xi-k* plant line, each exhibited an ~2-d flowering delay compared with the Columbia control (although the statistical significance of this delay was variable, depending on the time of measurement; see Supplemental Data Set 3 online). Examination of the synthetic mutants revealed additional flowering delays of 2 and 5 d for the *xi-k myob1 myob2 myob3* and *xi-k myob1 myob2 myob3 myob4* lines, compared with their respective 3KO and 4KO controls (Figure 6C; see Supplemental Data Set 3 online), and a dramatic 1-week delay relative to Columbia plants (Figures 6C and 6D).

Therefore, simultaneous inactivation of myosin XI-K and three or four of its MyoB interaction partners resulted in progressive defects in plant growth and flowering onset, implying shared functions of these proteins in plant development. It should be stressed that the phenotypes of the multiple *myob1-4* knockout mutants and synthetic multiple myosin *xi-k myob1-4* knockout mutants partially phenocopy those of the triple and quadruple

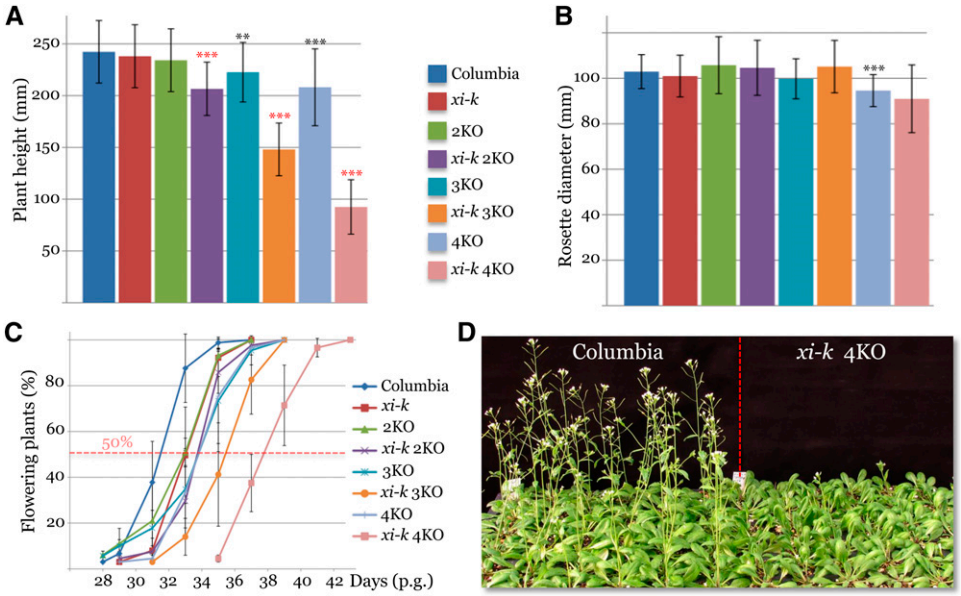

Figure 6. Growth and Flowering Phenotypes of the *Arabidopsis* Gene Knockout Plants in Which One to Five MYOB and/or Myosin XI-K Genes Were Inactivated.

(A) Mean plant height and SD (n = 36) at 38 d after germination. 2KO, *myob2 myob3*; 3KO, *myob1 myob2 myob3*; 4KO, *myob1 myob2 myob3 myob4*.
(B) Mean rosette diameter and SD (n = 36) at 38 d after germination.
(C) Time course of plant flowering measured as a percentage of flowering plants at each time point postgermination (p.g.). The time difference in flowering was quantified by comparing the times at which 50% of all plants of a given line had flowered (dotted red line).
(D) Image of a flat in which Columbia and *xi-k* 4KO (*xi-k myob1 myob2 myob3 myob4*) plants were grown next to each other for 35 d after germination. Asterisks indicate significance limits: **P < 0.01 and ***P < 0.001; black is for comparison with the Columbia control, whereas red is for controls corresponding to each synthetic mutant (*xi-k* 2KO versus 2KO; *xi-k* 3KO versus 3KO; and *xi-k* 4KO versus 4KO).

myosin XI mutants (Peremyslov et al., 2010), further supporting the functional interdependence of myosins XI and their MyoB receptors.

DISCUSSION

This work identifies core myosin receptors of transport vesicles in plants, a goal that so far proved elusive in yeast and vertebrate models. Furthermore, our results provide critical inroads into one of the most prominent but enigmatic phenomena in plant cell biology, the vigorous cytoplasmic streaming that has been known for a century but neither the biological role nor the mechanism of which so far has been experimentally characterized (Shimmen, 2007).

Our starting point was a Y2H screen for myosin XI interactors using the cargo binding GTDs of the principal *Arabidopsis* myosin XI-K as the bait. This screen netted three myosin binding candidates dubbed MyoB1-3 and represented by homologous proteins that possess the DUF593 domain (Figure 1A). In vitro pull-down assays validated the interactions between MyoB and myosins and demonstrated that DUF593 was sufficient for myosin binding (Figures 1B and 1D), suggesting that the main function of this domain is to interact with the myosins XI. Likewise, co-immunoprecipitation assays confirmed MyoB interactions with myosin XI-K in vivo (Figure 1C). Because additional Y2H screens revealed MyoB1 and MyoB2 interactions with myosin XI-1, as well as MyoB7 interaction with myosin XI-I, it seems likely that binding distinct subsets of DUF593-containing proteins is a common property of plant myosins XI.

Strikingly, the real-time imaging showed a virtually precise colocalization of MyoB1-GFP with myosin XI-K:mCherry (Figure 4A), both of which were associated with the motile vesicle-like bodies previously shown to be the principal cargo of myosin XI-K (Peremyslov et al., 2012). Similar to myosin-decorated vesicles, the MyoB1-YFP– or MyoB2-YFP–tagged vesicles moved in linear patterns in leaf or root epidermal cells and were concentrated in the apical domes of root hairs (Figure 2), a region of extensive secretion that drives polarized elongation (Cole and Fowler, 2006). We also found that myosin XI-K comigrated with MyoB1-GFP in Suc density gradient (see Supplemental Figure 3 online) and that, similar to myosin, nearly the entire intracellular pool of MyoB1 was associated with the microsomal membranes (Figure 2E). Moreover, the TM domain of MyoB1 was sufficient for targeting the YFP reporter to the motile vesicles (see Supplemental Figure 2 online).

Additional evidence of the functional relevance of the MyoB–myosin interaction was obtained using myosin gene knockout plants in which the MyoB1-YFP–tagged material appeared as diffuse immotile formations rather than linear arrays of motile vesicles that were observed in the Columbia plants (Figure 3A).

The FRAP analysis supported this conclusion by demonstrating only marginal FRAP values in knockout plants in contrast with the rapid recovery in Columbia plants (Figures 3B and 3C). The measurements of the vesicle velocity in the wild-type plants yielded an ~6.3 μm/s value that was very close to the ~7 μm/s velocity reported for myosin XI in biophysical experiments (Tominaga et al., 2003). This fastest known processive movement (exceeding the myosin V–dependent velocity 10-fold) (Tominaga and Nakano, 2012) further confirmed the myosin XI–driven mechanism of the MyoB vesicle transport.

The genetic interactions between myosin XI-K and MyoB1-4 revealed in synthetic gene knockout experiments firmly establish the functional significance of the cooperation between this myosin and MyoB1-4 (Figure 6). Importantly, the developmental defects of the synthetic quintuple (*xi-k myob1 myob2 myob3 myob4*) mutant partially phenocopied the quadruple (*xi-k xi-1 xi-2 xi-i*) myosin XI mutant (Peremyslov et al., 2010). Indeed, the height of the plants was reduced by two-thirds and their flowering delayed by approximately 1 week in both cases. However, the diameter of the leaf rosette was barely affected in the synthetic *myob* mutant, whereas it was substantially reduced in the myosin quadruple knockout line. These differences could be explained by the fact that MyoB1-4 proteins all belong to the same family I of the diverse superfamily of DUF593-containing proteins (Figure 5), whereas four myosins involved in our previous analysis represent three distinct evolutionary lineages (Peremyslov et al., 2011). In other words, there is no one-to-one relationship among functionally cooperating myosins and MyoB receptors; instead, myosins and their receptors probably form a network of functional interactions distinct parts of which are responsible for different functions.

Thus, we showed that MyoB1 interacts with myosins, colocalizes with myosins, is distributed in different cell types similarly to myosins, and moves in a myosin-dependent manner with a velocity typical of myosins XI. We also obtained solid genetic evidence of the functional cooperation between myosin XI-K and MyoB1-4 that is required for normal plant development. Collectively, these results demonstrate that MyoB proteins of family I are bona fide myosin receptors. Although more limited, the data on MyoB7 imaging and interaction with myosin XI-I suggest that family II DUF593-containing proteins also localize to motile vesicles that, however, are less abundant than vesicles defined by MyoB1 and MyoB2. It will be interesting to determine if family III proteins have yet another distinct localization pattern and functional profile as implied by the ER association of Floury1 in maize (Holding et al., 2007).

The two most important problems raised by this study are the identity and function of the vesicles defined by the myosin–MyoB interactions. To approach the former problem, we investigated the relationships between the MyoB-containing vesicles and several major endomembrane compartments. These analyses showed only marginal overlap between the vesicle-like material associated with MyoB1 and several distinct exocytic and endocytic compartments. Indeed, BFA treatment that affects ER-Golgi interface and post-Golgi vesicle transport had no detectable effect on MyoB1-tagged vesicles (Figure 4C). The secretory pathways defined by Golgi, SCAMP2 (Peremyslov et al., 2012), or VAMP721 (Figure 4B), as well as clathrin- and flotillin-dependent exocytic pathways (Figures 4D and 4E, respectively), showed only minimal (if any) colocalization with myosin XI-K:YFP or MyoB1-GFP. The myosin XI-K– and MyoB1-decorated membranes were confidently separated from PVC, also known as multivesicular body, where the endocytic and exocytic pathways converge (see Supplemental Figure 3 online) (Foresti and Denecke, 2008; Richter et al., 2009; Scheuring et al., 2011; Contento and Bassham, 2012). These findings present a striking contrast to the nearly perfect colocalization of MyoB1-GFP with myosin XI-K:mCherry (Figure 4A). Collectively, these results imply that the interaction between myosin XI-K and MyoB1 (and presumably the interactions between myosins XI and MyoB in general) define a distinct class of transport vesicles.

What is the function(s) of the vesicles mobilized by the myosin–MyoB interactions? As previously established by multiple lines of evidence, myosin XI-K provides major contributions to the diffuse and polarized cell growth, suggesting an important role of this motor in the delivery of secretory vesicles to the regions of growth and/or membrane recycling (Ojangu et al., 2007; Peremyslov et al., 2008, 2010, 2012; Prokhnevsky et al., 2008). Given that the MyoB-decorated vesicles are the major cargo of a principal myosin, it appears likely that these vesicles are involved in a key exocytic and/or endocytic pathway. This possibility seems to be further supported by the abolishment of trafficking of the SCAMP2- (Peremyslov et al., 2012) and MyoB1-tagged vesicles (Figure 3) in the triple myosin knockout plants, as well as by freezing of the endomembrane traffic in quadruple myosin knockout plants (Peremyslov et al., 2010). Unexpectedly, we found no relationship between several known endomembrane compartments and the transport pathway defined by the MyoB-myosin vesicles.

Moreover, there is a stark contrast in the intracellular distribution and motility patterns between the previously described types of vesicles and organelles on the one hand and the MyoB-decorated vesicles on the other hand. The Golgi stacks, peroxisomes, mitochondria, and ER each are distributed over the cortical cytoplasm, including association with the F-actin network, unlike the MyoB vesicles that are predominantly confined to this network. Organelles also exhibit a range of motility patterns from immobile to slow movement over short distances to rapid movement over long distances (Nebenführ et al., 1999; Avisar et al., 2008; Zheng et al., 2009). Similar patterns were observed for the vesicles, for instance, those tagged by SCAMP2 (Peremyslov et al., 2012), the *trans*-Golgi network, PVC and endosomes (Avisar et al., 2012), or the clathrin light chain (see Supplemental Movie 8 online). By contrast, the vesicles associated with myosin XI-K and MyoB1-2 (or myosin XI-I and MyoB7) exhibit continuous movement with a mean velocity that is significantly higher than the velocity of the organelles (see Supplemental Movies 1 to 3 online).

Taken together, these findings present an apparent paradox. Although the motility of organelles, SCAMP2 vesicles, the *trans*-Golgi network, the PVC, endosomes, and the entire cytoplasmic streaming defined as the sum total of endomembrane trafficking depend entirely on myosins XI (Peremyslov et al., 2010; Avisar et al., 2012), the principal one among them, myosin XI-K, does not colocalize with these organelles or vesicles (Peremyslov et al., 2012). The myosin XI-K GTD that exerts a dominant-negative

inhibition effect on the transport of multiple organelles and vesicle types also does not overlap with these endomembranes (Avisar et al., 2012). Instead, myosin XI-K is attached to MyoB-tagged vesicles that move in a continuous and rapid manner distinct from the slower saltatory movement of organelles and several major types of vesicles.

The simplest solution to this paradox is that MyoB vesicles are actively moved by myosins XI, whereas the organelles and other vesicles are moved passively. In other words, the vesicles decorated by MyoB and myosin XI constitute a specialized transport system akin to a conveyer or a skiing rope tow, whereas organelles and carrier vesicles are dragged along, either by transiently clamping to MyoB vesicles or merely by following their hydrodynamic flow. The working model in Figure 7 proposes that MyoB proteins act as membrane-anchored core myosin receptors, possibly aided by adaptors such as Rab GTPases, which are the membrane identity determinants implicated in binding myosins V and XI (Hashimoto et al., 2008; Hammer and Sellers, 2012). This model provides a framework for further inquiry into the mechanisms of myosin-dependent endomembrane transport and eventually for addressing the biological role of cytoplasmic streaming in plants.

An alternative albeit less parsimonious solution to the above paradox is transient association of the MyoB myosin receptors with subpopulations of various carrier vesicles or organelles that renders them transport competent. Accordingly, the entire pool of MyoB-positive vesicles could be a combination of many different endomembrane compartments engaged in active transport. Testing these or other possible models will be aided by (1) functional inactivation of the MyoB subsets (Figure 6) followed by investigation of the transport competence of distinct vesicle types; (2) identification of the composition and cargo of the MyoB vesicles; and (3) characterization of the protein–protein interaction networks that involve MyoB and myosins XI. It also will be important to determine the functions of the DUF593 superfamily members in other plant species, including crop plants used as major sources of food, fiber, and biofuel. The groundbreaking work on the *Floury1* gene, which contributes to seed development in maize, is testimony to the versatility of the biological functions of this protein superfamily (Holding et al., 2007).

The importance of the DUF593 superfamily in plant biology and evolution is further emphasized by its universal conservation, proliferation, and structural diversification in the land plants (Figure 5). The multidomain organization of the DUF593-containing proteins suggests that they are involved in multiple protein–protein interactions. In addition to the principal myosin receptor function provided by the TM and DUF593 domains, such interactions (e.g., via the MBRs) could regulate myosin-dependent vesicular transport. Furthermore, it is notable that the DUF593 and myosin XI multigene families in plants show similar extents of diversification (13 and 15 genes, respectively, in *Arabidopsis*) and a similar number of (sub)families (five for the myosin XI family and six for the DUF593-containing proteins). In both cases, the diversification of the (sub)families appears to be traceable to the stem phase of land plant evolution. Furthermore, the gene expression profiles of both myosin XI genes and DUF593 protein–coding genes can be partitioned into those that are broadly expressed in a vegetative plant (sporophyte) and those that are specifically restricted to pollen (gametophyte) (see Supplemental Figure 5 online) (Peremyslov et al., 2011).

In conclusion, the discovery of the transport system that relies on myosins XI and MyoB receptors provides an advanced model to characterize the vesicle transport in a multicellular eukaryote (Figure 7). Although this system involves plant-specific MyoB components, analogous membrane-anchored receptors for

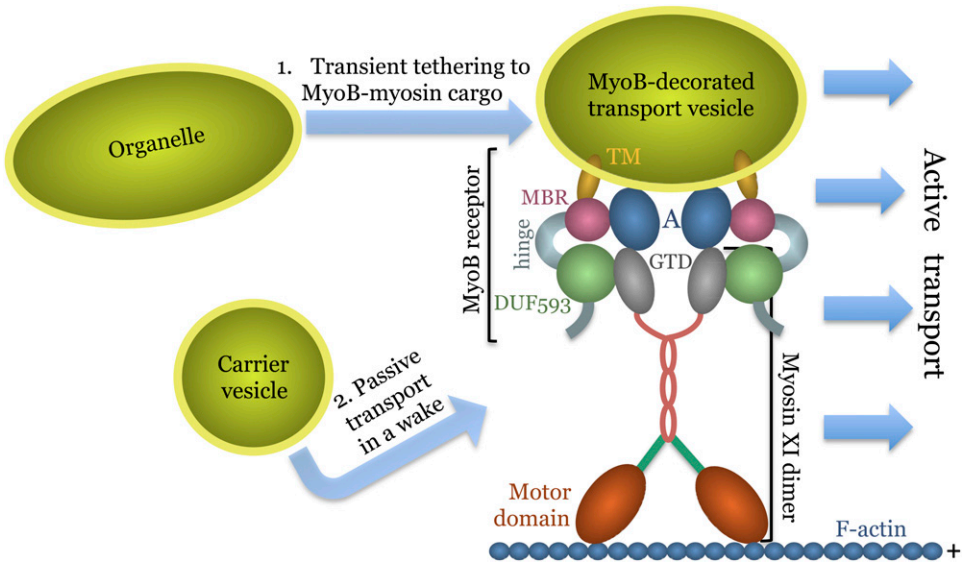

Figure 7. Model of a Transport Vesicle Attachment to Myosin XI via Interaction with a Primary MyoB Receptor and a Hypothetical Adaptor A (e.g., Rab GTPase).

The hypothetical mechanisms whereby other endomembranes are mobilized by the specialized, MyoB-containing, transport vesicles are shown at the left.

myosins V are likely to exist in fungi and animals as implied by an ongoing search for the PI4P-dependent factor X that is required for myosin V–driven transport of vesicles in yeast (Santiago-Tirado et al., 2011; Donovan and Bretscher, 2012).

METHODS

Y2H Analysis

The Y2H analysis was based on the Matchmaker GAL4-based assay (Clontech). The cDNAs encoding GTDs of *Arabidopsis thaliana* myosin XI-K (amino acid residues Thr-1058 to Ser1531), XI-1 (Thr-1048 to Asp-1520), and XI-I (Ile-1059 to Ile-1522) (Peremyslov et al., 2011) were cloned into pGBKT7 bait plasmid and introduced into Y2H Gold yeast strain. Testing for autoactivation and toxicity of the GTD was performed according to the manufacturer's protocols. A Mate and Plate Normalized *Arabidopsis* Universal Library (Clontech) was used for mating, and screening was performed on SD medium lacking Leu, Trp, and His and supplemented with 10 mM 3-amino-1,2,4-triazole. After 7 d at 30°C, growing yeast colonies were streaked on SD/-Leu/-Trp/-His/-Ade medium containing X-α-Gal. Colonies that turned blue in the presence of the chromogenic substrate were grown in liquid SD/-Leu/-Trp/-His/-Ade medium, and plasmids were isolated and sequenced. In addition, GTD cDNAs of the myosin XI-1 and XI-I were cloned into the pGBKT7 and cotransformed with the prey plasmids harboring MyoB1 and MyoB2 cDNAs into Y2H Gold yeast strain and plated as described above. GFP fused to the GAL4 activation domain was used as a negative control for the interaction tests.

Pull-Down and Coimmunoprecipitation Assays

The myosin XI-K GTD cDNA or a GUS cDNA was subcloned into a pMAL vector as fusions with MBP (New England Biolabs) and introduced into the *Escherichia coli* BL21(DE3)LysS strain. Expression of the fusion proteins was induced by isopropylthio-β-galactoside (0.5 mM) at 28°C for 6 h. Cells were resuspended in PBS containing 0.5% Triton X-100, 2 mM EDTA, 1 mM phenylmethylsulfonyl fluoride, and 1× Complete Protease Inhibitor Cocktail (Roche Applied Science), freeze-thawed, sonicated, and centrifuged (16,000*g*, 4°C). Supernatants were incubated with Amylose resin (New England Biolabs) for 1 h and washed with the same buffer. Partial cDNAs of MyoB2 ORF encoding putative TM and MBRs (TM-MBR) (amino acid residues 1 to 169) or DUF593 (residues 399 to 536) were subcloned in frame with the GFP cDNA in a pMDC32 binary plasmid using *Asc*I and *Pac*I sites. A GFP-GUS hybrid cDNA or a GFP cDNA were cloned into pMDC32 and used as interaction negative controls. *Nicotiana benthamiana* leaves were infiltrated with *Agrobacterium tumefaciens* strain GV3101 transformed with the binary vectors and kept for 2 d in the greenhouse. Leaves were ground in 3 volumes of 20 mM HEPES, pH 7.2, 50 mM potassium acetate, 1 mM EDTA, 1 mM EGTA, 5% glycerol, 1% Triton X-100, 1 mM DTT, 1 mM phenylmethylsulfonyl fluoride, and 1× Complete Protease Inhibitor Cocktail on ice. Homogenates were centrifuged at 8000*g* for 10 min, mixed with the MBP fusion protein loaded Amylose beads, incubated with slow shaking for 1 h, washed, and boiled in SDS sample buffer. For the coimmunoprecipitation assay, the YFP-tagged MyoB1 was transiently expressed in *N. benthamiana*. Plant extracts were incubated with the agarose-immobilized anti-GFP rat monoclonal antibodies (Medical and Biological Laboratories) for 1 h on ice. After washes, the beads were boiled in SDS sample buffer, and bound proteins were resolved in a 10% SDS-PAGE and detected by immunoblotting using anti-GFP rabbit polyclonal antibody (Rockland Immunochemicals) or myosin XI-K–specific antibody (Peremyslov et al., 2008).

Expression of Fluorophore-Tagged Proteins

A 5580-bp-long genomic fragment encompassing the *MYOB1* (*At1g08800*) gene and its putative promoter was PCR amplified from the genomic DNA using KOD Hot Start high-fidelity DNA polymerase (Novagen) and cloned into a modified pMDC32 plasmid using the *Sbf*I and *Pac*I sites. The YFP cDNA was added downstream from MyoB1 ORF to yield a pMDC-gAt1g08800-YFP. This plasmid was mobilized into *Agrobacterium* GV3101 for floral dipping transformation of *Arabidopsis* Columbia plants, as well as the *myob1* knockout line (SALK_150594), *xi-k* knockout line (SALK_067972)(Peremyslov et al., 2008), and *xi-k xi-1 xi-2* triple knockout plants (Peremyslov et al., 2010). Likewise, a 4452-bp-long genomic segment encompassing the *MyoB2* (*At1g70750*) and the upstream promoter region was cloned to obtain pMDC-gAt1g70750-YFP that was used to transform Columbia and the *myob2* knockout plant line (SALK_029986). Analogously, a 3938-bp genomic fragment of *MYOB7* (*At5g06560*), including its native promoter, was cloned into a pMDC32 plasmid. A GFP ORF was added upstream from the MyoB7 ORF, and the resulting pMDC-GFP-gAt5g06560 plasmid was used to transform Columbia-0 plants.

To generate a dual MyoB1-GFP/XI-K:mCherry expression vector, a GFP cDNA was substituted for the YFP cDNA in the pMDC-gAt1g08800-YFP. An entire GFP-tagged genomic copy of *MyoB1* was amplified using high-fidelity DNA polymerase from *Thermococcus kodakaraensis* (KOD1) and cloned into a unique *Mau*BI site of the pMDC carrying a mCherry-tagged genomic copy of the *Arabidopsis XI-K* gene (Peremyslov et al., 2012). A resulting plasmid was used to transform myosin triple knockout plants. To generate a marker of exocytic vesicles, a genomic copy of the v-SNARE VAMP721 (*AT1G04750*) (Zhang et al., 2011), including its native promoter, was PCR amplified and the mCherry ORF was added before the first codon of the VAMP721 ORF using overlapping PCRs. The resulting construct was cloned into pMDC32 using *Sbf*I and *Pac*I sites. To visualize clathrin-coated endocytic vesicles, a genomic copy of *Arabidopsis* clathrin light chain (*AT2G40060*) including its promoter was fused to mCherry and cloned to pMDC32 as described above. A marker of clathrin-independent endocytosis, *Arabidopsis* Flotillin1 (*AT5G25250*) (Li et al., 2012) was fused to mCherry and placed under control of a 35S promoter using *Asc*I and *Pac*I sites of pMDC32. An expression cassette for the GFP-tagged genomic *MyoB1* was added to these plasmids using the unique *Mau*BI site, and the resulting dual-cassette plasmids were used to transform the *myob1* knockout line.

BFA Treatments, CLSM, and FRAP

Arabidopsis seedlings expressing fluorophore-tagged proteins were treated with 50 μM BFA for 2 h, and the BFA-sensitive endomembrane compartments were imaged using the following markers: Golgi markers N-acetylglucosaminyl transferase fused to GFP (NAG-GFP) (Grebe et al., 2003) and Golgi-resident rat sialyl transferase (ST-YFP), a cyan fluorescent protein–tagged ER marker (Brandizzi et al., 2002), YFP-AtRabA4b, a marker of the *trans*-Golgi network to plasma membrane trafficking pathway (Preuss et al., 2004). Multicolor observation was performed using an LSM510 Meta confocal microscope (Carl Zeiss). GFP, YFP, and mCherry were excited with 488- or 514-nm argon laser lines or a 561-nm HeNe laser line, respectively. The fluorescence emission spectra were collected through a band-pass 505- to 530-nm (GFP), band-pass 530- to 600-nm (YFP), or band-pass 560- to 615-nm (mCherry) filter. For the simultaneous visualization of two fluorophores, dual channel acquisition of the GFP and mCherry signal was done sequentially to minimize crosstalk. In each imaging analysis, over 20 different cells from at least five leaves were screened. The images shown in Figures 2 to 4 are representative of over 90% of the screened cells. The microscopy setup for FRAP measurements was described previously (Peremyslov et al., 2012). Briefly, both argon (all lines) and diode 405-nm lasers were used at

maximum output power for 8 s to bleach a defined region of a cell. Recovery was monitored at 5% argon laser intensity as time series (18 frames over 30-s recovery time). Two identical regions of interest were monitored: One was inside and one was outside of the bleached area. The fluorescence in the regions of interest was quantified using Zeiss LSM software. Each FRAP value shown in Figure 3B corresponds to a mean and SD from 10 distinct measurements.

Subcellular Fractionation

pMDC-gAt1g08800-YFP described above was used to produce transgenic *Arabidopsis* plants by the floral dipping method (Clough and Bent, 1998). T2 seeds were plated onto half-strength Murashige and Skoog medium supplemented with 2% Suc, 0.6% Phytagel, and 25 μg/mL hygromycin, and plants were grown for 2 weeks under normal growth conditions (23°C, 16 h light/8 h dark). Plant homogenates were prepared as described (Zhang et al., 2010). A 1000 g supernatant was centrifuged at 100,000*g* for 1 h with or without the addition of 1% Triton X-100. Suc density gradient fractionation was performed as described (Peremyslov et al., 2012); a separation pattern shown in Supplemental Figure 3 online is representative of four independent experiments.

Sequence and Phylogenetic Analysis

The PSI-BLAST (Altschul et al., 1997) search (with an inclusion threshold *E*-value = 10^{-4}, low complexity masking, and composition-based statistics off) with a query sequence corresponding to the DUF593 domain region (402 to 515 amino acids) of *At1g70750* against the Refseq database (Pruitt et al., 2007) was used to identify the proteins containing the DUF593 domain. The MUSCLE program with default parameters (Edgar, 2004) was used to construct a multiple sequence alignment of the DUF593 domain. Identical and incomplete sequences were discarded prior to further analysis. Altogether, 172 nonredundant sequences were further analyzed. The maximum likelihood phylogenetic tree was constructed using the RAxML program, with the WAG substitution matrix and gamma-distributed evolutionary rates (Stamatakis, 2006); the bootstrap support was computed over 1000 replications using the extended majority rule. Search for conserved protein domains was performed using the RPS-BLAST program (Altschul et al., 1997). The Trans Membrane Hidden Markov Model (Sonnhammer et al., 1998) and Marcoil (Delorenzi and Speed, 2002) programs with default parameters were used for the prediction of transmembrane helices and coiled-coil regions, respectively.

Gene Knockout Lines and Phenotypic Analysis

The T-DNA insertion mutants in the Columbia-0 background were obtained from the SALK collection, and the homozygous mutants were identified by PCR-based genotyping using allele-specific primers. The following lines were analyzed: SALK_150594 (*myob1*), SALK_029986 (*myob2*), SALK_138222 (*myob3*), and SALK_144108 (*myob4*). The insertion sites were confirmed by DNA sequencing of the border fragments. Absence of correct transcripts in each of the mutants was confirmed by endpoint RT-PCR on total RNA (see Supplemental Figure 6 online).

To generate multiple homozygous mutants containing null alleles of the MyoB family I, the single mutants *myob1*, *myob2*, *myob3*, and *myob4* were crossed to generate higher order knockouts *myob2 myob3*, *myob1 myob2 myob3*, and *myob1 myob2 myob3 myob4*, respectively. The *xi-k* homozygous line SALK_067972 described previously (Peremyslov et al., 2008) was used to obtain *xi-k myob2 myob3*, *xi-k myob1 myob2 myob3*, and *xi-k myob1 myob2 myob3 myob4* lines.

For the phenotypic analysis, plants were grown in 72-well flats, with 36 wells for each mutant. Five identical replicas of each flat were planted simultaneously and arranged randomly in the greenhouse. Flats were shuffled daily to compensate for local variations in the growth conditions. The daylength was 12 h, and daytime and nighttime temperatures were maintained at 22 and 20°C, respectively. The following parameters were logged: flowering time (defined here as the expansion of petals on the first flower and recorded daily) and plant height and rosette diameter measured at day 38 after germination. The statistical analysis was performed using the nonparametric Wilcoxon Mann-Whitney test (see Supplemental Data Set 3 online).

Accession Numbers

Sequence data from this article can be found in the Arabidopsis Genome Initiative or GenBank/EMBL databases under the following accession numbers: At1go8800 (MyoB1), At1g70750 (MyoB2), At5g16720 (MyoB3), At2g30690 (MyoB4), At5g06560 (MyoB7), At1g04750 (VAMP721), AT2G40060 (CLC), and At5g25250 (Flotillin1).

Supplemental Data

The following materials are available in the online version of this article.

Supplemental Figure 1. Pairwise Yeast Two-Hybrid Assays Validating Interactions between the Globular Tail Domains of the Myosins XI-1 and XI-I and the MyoB Proteins.

Supplemental Figure 2. The N-Terminal Transmembrane Region of MyoB2 Is Sufficient for Targeting GFP Reporter to Motile Vesicles.

Supplemental Figure 3. Cell Fractionation Analysis of the Distribution of MyoB2-YFP Using Suc Gradient (20 to 60%) Centrifugation and Immunoblotting of the *Arabidopsis myob1 MyoB1-YFP* Extracts.

Supplemental Figure 4. Phylogenetic Trees of DUF593-Containing Proteins.

Supplemental Figure 5. Developmental- and Anatomy-Specific Expression Profiles of *Arabidopsis* DUF593-Containing Proteins.

Supplemental Figure 6. The RT-PCR Analysis of the Gene Expression in the Homozygous T-DNA Insertion Lines SALK_150594 (*myob1*), SALK_029986 (*myob2*), SALK_138222 (*myob3*), and SALK_144108 (*myoB4*) Compared with Columbia Controls as Indicated.

Supplemental Data Set 1. Results of Sequence Analysis of the Proteins Containing Complete DUF593 Domain.

Supplemental Data Set 2. Complete Alignment of DUF593-Containing Proteins Detected by PSI-BLAST.

Supplemental Data Set 3. Statistical Analysis of the Mutant Phenotypes.

Supplemental Movie 1. Traffic of the MyoB1-YFP–Tagged Vesicular Bodies in the *Arabidopsis myob1 MyoB1-YFP* Leaf Epidermal Cell.

Supplemental Movie 2. Traffic of the MyoB2-YFP-Tagged Vesicular Bodies in the *Arabidopsis myob2 MyoB2-YFP* Leaf Epidermal Cell.

Supplemental Movie 3. Traffic of the YFP-MyoB7–Tagged Vesicular Bodies in the *Arabidopsis YFP-MyoB7* Leaf Epidermal Cell.

Supplemental Movie 4. Traffic of the MyoB1-YFP–Tagged Vesicular Bodies in the *Arabidopsis xi-k MyoB1-YFP* Leaf Epidermal Cell.

Supplemental Movie 5. The MyoB1-YFP–Tagged Material in the *Arabidopsis xi-k xi-1 xi-2 MyoB1-YFP* Leaf Epidermal Cell.

Supplemental Movie 6. Fluorescence Recovery after Photobleaching Assay in the *Arabidopsis MyoB1-YFP* Leaf Epidermal Cell.

Supplemental Movie 7. Fluorescence Recovery after Photobleaching Assay in the *Arabidopsis xi-k xi-1 xi-2 MyoB1-YFP* Leaf Epidermal Cell.

Supplemental Movie 8. Traffic of the CLC2:mCherry-Tagged Clathrin-Coated Vesicles in the Marker-Transformed *Arabidopsis* Columbia Plants.

Supplemental Movie Legends 1. Legends for Supplemental Movies 1-8.

ACKNOWLEDGMENTS

We thank David Taylor and Valerie Fraser for excellent technical assistance. The initial stage of this work was supported by National Institutes of Health Award R01 GM087658 to V.V.D. K.S.M and E.V.K. are supported by intramural funds of the U.S. Department of Health and Human Services (to the National Library of Medicine).

AUTHOR CONTRIBUTIONS

V.V.D., V.V.P., E.V.K., and K.S.M. designed the research. V.V.P., E.A.M., E.G.K. and K.S.M. performed the research. V.V.D. and E.V.K. wrote the article.

Received May 13, 2013; revised June 22, 2013; accepted August 8, 2013; published August 30, 2013.

REFERENCES

Altschul, S.F., Madden, T.L., Schäffer, A.A., Zhang, J., Zhang, Z., Miller, W., and Lipman, D.J. (1997). Gapped BLAST and PSI-BLAST: A new generation of protein database search programs. Nucleic Acids Res. **25:** 3389–3402.

Aravind, L., Iyer, L.M., and Koonin, E.V. (2006). Comparative genomics and structural biology of the molecular innovations of eukaryotes. Curr. Opin. Struct. Biol. **16:** 409–419.

Avisar, D., Abu-Abied, M., Belausov, E., and Sadot, E. (2012). Myosin XIK is a major player in cytoplasm dynamics and is regulated by two amino acids in its tail. J. Exp. Bot. **63:** 241–249.

Avisar, D., Abu-Abied, M., Belausov, E., Sadot, E., Hawes, C., and Sparkes, I.A. (2009). A comparative study of the involvement of 17 Arabidopsis myosin family members on the motility of Golgi and other organelles. Plant Physiol. **150:** 700–709.

Avisar, D., Prokhnevsky, A.I., Makarova, K.S., Koonin, E.V., and Dolja, V.V. (2008). Myosin XI-K Is required for rapid trafficking of Golgi stacks, peroxisomes, and mitochondria in leaf cells of *Nicotiana benthamiana*. Plant Physiol. **146:** 1098–1108.

Bonifacino, J.S., and Glick, B.S. (2004). The mechanisms of vesicle budding and fusion. Cell **116:** 153–166.

Brandizzi, F., and Barlowe, C. (2013). Organization of the ER-Golgi interface for membrane traffic control. Nat. Rev. Mol. Cell Biol. **14:** 382–392.

Brandizzi, F., Snapp, E.L., Roberts, A.G., Lippincott-Schwartz, J., and Hawes, C. (2002). Membrane protein transport between the endoplasmic reticulum and the Golgi in tobacco leaves is energy dependent but cytoskeleton independent: Evidence from selective photobleaching. Plant Cell **14:** 1293–1309.

Brandizzi, F., and Wasteneys, G.O. (2013). Cytoskeleton-dependent endomembrane organization in plant cells: An emerging role for microtubules. Plant J. **75:** 339–349.

Bryant, D.M., Datta, A., Rodríguez-Fraticelli, A.E., Peränen, J., Martín-Belmonte, F., and Mostov, K.E. (2010). A molecular network for de novo generation of the apical surface and lumen. Nat. Cell Biol. **12:** 1035–1045.

Chardin, P., and McCormick, F. (1999). Brefeldin A: The advantage of being uncompetitive. Cell **97:** 153–155.

Chen, X., Irani, N.G., and Friml, J. (2011). Clathrin-mediated endocytosis: The gateway into plant cells. Curr. Opin. Plant Biol. **14:** 674–682.

Clough, S.J., and Bent, A.F. (1998). Floral dip: A simplified method for *Agrobacterium*-mediated transformation of *Arabidopsis thaliana*. Plant J. **16:** 735–743.

Cole, R.A., and Fowler, J.E. (2006). Polarized growth: Maintaining focus on the tip. Curr. Opin. Plant Biol. **9:** 579–588.

Contento, A.L., and Bassham, D.C. (2012). Structure and function of endosomes in plant cells. J. Cell Sci. **125:** 3511–3518.

Delorenzi, M., and Speed, T. (2002). An HMM model for coiled-coil domains and a comparison with PSSM-based predictions. Bioinformatics **18:** 617–625.

Donovan, K.W., and Bretscher, A. (2012). Myosin-V is activated by binding secretory cargo and released in coordination with Rab/exocyst function. Dev. Cell **23:** 769–781.

Edgar, R.C. (2004). MUSCLE: A multiple sequence alignment method with reduced time and space complexity. BMC Bioinformatics **5:** 113.

Fagarasanu, A., Mast, F.D., Knoblach, B., and Rachubinski, R.A. (2010). Molecular mechanisms of organelle inheritance: Lessons from peroxisomes in yeast. Nat. Rev. Mol. Cell Biol. **11:** 644–654.

Foresti, O., and Denecke, J. (2008). Intermediate organelles of the plant secretory pathway: Identity and function. Traffic **9:** 1599–1612.

Foth, B.J., Goedecke, M.C., and Soldati, D. (2006). New insights into myosin evolution and classification. Proc. Natl. Acad. Sci. USA **103:** 3681–3686.

Grebe, M., Xu, J., Möbius, W., Ueda, T., Nakano, A., Geuze, H.J., Rook, M.B., and Scheres, B. (2003). *Arabidopsis* sterol endocytosis involves actin-mediated trafficking via ARA6-positive early endosomes. Curr. Biol. **13:** 1378–1387.

Hammer, J.A., III., and Sellers, J.R. (2012). Walking to work: Roles for class V myosins as cargo transporters. Nat. Rev. Mol. Cell Biol. **13:** 13–26.

Hashimoto, K., Igarashi, H., Mano, S., Takenaka, C., Shiina, T., Yamaguchi, M., Demura, T., Nishimura, M., Shimmen, T., and Yokota, E. (2008). An isoform of *Arabidopsis* myosin XI interacts with small GTPases in its C-terminal tail region. J. Exp. Bot. **59:** 3523–3531.

Holding, D.R., Otegui, M.S., Li, B., Meeley, R.B., Dam, T., Hunter, B.G., Jung, R., and Larkins, B.A. (2007). The maize floury1 gene encodes a novel endoplasmic reticulum protein involved in zein protein body formation. Plant Cell **19:** 2569–2582.

Ito, Y., Uemura, T., Shoda, K., Fujimoto, M., Ueda, T., and Nakano, A. (2012). cis-Golgi proteins accumulate near the ER exit sites and act as the scaffold for Golgi regeneration after brefeldin A treatment in tobacco BY-2 cells. Mol. Biol. Cell **23:** 3203–3214.

Jin, Y., Sultana, A., Gandhi, P., Franklin, E., Hamamoto, S., Khan, A.R., Munson, M., Schekman, R., and Weisman, L.S. (2011). Myosin V transports secretory vesicles via a Rab GTPase cascade and interaction with the exocyst complex. Dev. Cell **21:** 1156–1170.

Kang, B.H., Nielsen, E., Preuss, M.L., Mastronarde, D., and Staehelin, L.A. (2011). Electron tomography of RabA4b- and PI-4Kβ1-labeled trans Golgi network compartments in *Arabidopsis*. Traffic **12:** 313–329.

Konopka, C.A., Backues, S.K., and Bednarek, S.Y. (2008). Dynamics of *Arabidopsis* dynamin-related protein 1C and a clathrin light chain at the plasma membrane. Plant Cell **20:** 1363–1380.

Li, J.F., and Nebenführ, A. (2008). The tail that wags the dog: The globular tail domain defines the function of myosin V/XI. Traffic **9:** 290–298.

Li, R., Liu, P., Wan, Y., Chen, T., Wang, Q., Mettbach, U., Baluska, F., Samaj, J., Fang, X., Lucas, W.J., and Lin, J. (2012). A membrane microdomain-associated protein, *Arabidopsis* Flot1, is involved in a clathrin-independent endocytic pathway and is required for seedling development. Plant Cell **24:** 2105–2122.

Lipatova, Z., Tokarev, A.A., Jin, Y., Mulholland, J., Weisman, L.S., and Segev, N. (2008). Direct interaction between a myosin V motor and the Rab GTPases Ypt31/32 is required for polarized secretion. Mol. Biol. Cell **19:** 4177–4187.

Matthews, J.M., and Sunde, M. (2002). Zinc fingers—Folds for many occasions. IUBMB Life **54:** 351–355.

Nebenführ, A., Gallagher, L.A., Dunahay, T.G., Frohlick, J.A., Mazurkiewicz, A.M., Meehl, J.B., and Staehelin, L.A. (1999). Stop-and-go movements of plant Golgi stacks are mediated by the acto-myosin system. Plant Physiol. **121:** 1127–1142.

Ojangu, E.L., Järve, K., Paves, H., and Truve, E. (2007). *Arabidopsis thaliana* myosin XIK is involved in root hair as well as trichome morphogenesis on stems and leaves. Protoplasma **230:** 193–202.

Pashkova, N., Jin, Y., Ramaswamy, S., and Weisman, L.S. (2006). Structural basis for myosin V discrimination between distinct cargoes. EMBO J. **25:** 693–700.

Peremyslov, V.V., Klocko, A.L., Fowler, J.E., and Dolja, V.V. (2012). *Arabidopsis* myosin XI-K localizes to the motile endomembrane vesicles associated with F-actin. Front. Plant Sci. **3:** 184.

Peremyslov, V.V., Mockler, T.C., Filichkin, S.A., Fox, S.E., Jaiswal, P., Makarova, K.S., Koonin, E.V., and Dolja, V.V. (2011). Expression, splicing, and evolution of the myosin gene family in plants. Plant Physiol. **155:** 1191–1204.

Peremyslov, V.V., Prokhnevsky, A.I., Avisar, D., and Dolja, V.V. (2008). Two class XI myosins function in organelle trafficking and root hair development in Arabidopsis. Plant Physiol. **146:** 1109–1116.

Peremyslov, V.V., Prokhnevsky, A.I., and Dolja, V.V. (2010). Class XI myosins are required for development, cell expansion, and F-Actin organization in *Arabidopsis*. Plant Cell **22:** 1883–1897.

Preuss, M.L., Serna, J., Falbel, T.G., Bednarek, S.Y., and Nielsen, E. (2004). The *Arabidopsis* Rab GTPase RabA4b localizes to the tips of growing root hair cells. Plant Cell **16:** 1589–1603.

Prokhnevsky, A.I., Peremyslov, V.V., and Dolja, V.V. (2008). Overlapping functions of the four class XI myosins in *Arabidopsis* growth, root hair elongation, and organelle motility. Proc. Natl. Acad. Sci. USA **105:** 19744–19749.

Pruitt, K.D., Tatusova, T., and Maglott, D.R. (2007). NCBI reference sequences (RefSeq): A curated non-redundant sequence database of genomes, transcripts and proteins. Nucleic Acids Res. **35** (Database issue)**:** D61–D65.

Richards, T.A., and Cavalier-Smith, T. (2005). Myosin domain evolution and the primary divergence of eukaryotes. Nature **436:** 1113–1118.

Richter, S., Voss, U., and Jürgens, G. (2009). Post-Golgi traffic in plants. Traffic **10:** 819–828.

Ritzenthaler, C., Nebenführ, A., Movafeghi, A., Stussi-Garaud, C., Behnia, L., Pimpl, P., Staehelin, L.A., and Robinson, D.G. (2002). Reevaluation of the effects of brefeldin A on plant cells using tobacco Bright Yellow 2 cells expressing Golgi-targeted green fluorescent protein and COPI antisera. Plant Cell **14:** 237–261.

Roland, J.T., Bryant, D.M., Datta, A., Itzen, A., Mostov, K.E., and Goldenring, J.R. (2011). Rab GTPase-Myo5B complexes control membrane recycling and epithelial polarization. Proc. Natl. Acad. Sci. USA **108:** 2789–2794.

Sanderfoot, A. (2007). Increases in the number of SNARE genes parallels the rise of multicellularity among the green plants. Plant Physiol. **144:** 6–17.

Sang, Y., Li, Q.H., Rubio, V., Zhang, Y.C., Mao, J., Deng, X.W., and Yang, H.Q. (2005). N-terminal domain-mediated homodimerization is required for photoreceptor activity of *Arabidopsis* CRYPTOCHROME 1. Plant Cell **17:** 1569–1584.

Santiago-Tirado, F.H., Legesse-Miller, A., Schott, D., and Bretscher, A. (2011). PI4P and Rab inputs collaborate in myosin-V-dependent transport of secretory compartments in yeast. Dev. Cell **20:** 47–59.

Scheuring, D., Viotti, C., Krüger, F., Künzl, F., Sturm, S., Bubeck, J., Hillmer, S., Frigerio, L., Robinson, D.G., Pimpl, P., and Schumacher, K. (2011). Multivesicular bodies mature from the trans-Golgi network/early endosome in *Arabidopsis*. Plant Cell **23:** 3463–3481.

Schott, D., Ho, J., Pruyne, D., and Bretscher, A. (1999). The COOH-terminal domain of Myo2p, a yeast myosin V, has a direct role in secretory vesicle targeting. J. Cell Biol. **147:** 791–808.

Schott, D.H., Collins, R.N., and Bretscher, A. (2002). Secretory vesicle transport velocity in living cells depends on the myosin-V lever arm length. J. Cell Biol. **156:** 35–39.

Schuh, M. (2011). An actin-dependent mechanism for long-range vesicle transport. Nat. Cell Biol. **13:** 1431–1436.

Shimmen, T. (2007). The sliding theory of cytoplasmic streaming: Fifty years of progress. J. Plant Res. **120:** 31–43.

Shimmen, T., and Yokota, E. (2004). Cytoplasmic streaming in plants. Curr. Opin. Cell Biol. **16:** 68–72.

Simons, K., and Gerl, M.J. (2010). Revitalizing membrane rafts: New tools and insights. Nat. Rev. Mol. Cell Biol. **11:** 688–699.

Smith, L.G., and Oppenheimer, D.G. (2005). Spatial control of cell expansion by the plant cytoskeleton. Annu. Rev. Cell Dev. Biol. **21:** 271–295.

Sonnhammer, E.L., von Heijne, G., and Krogh, A. (1998). A hidden Markov model for predicting transmembrane helices in protein sequences. Proc. Int. Conf. Intell. Syst. Mol. Biol. **6:** 175–182.

Stamatakis, A. (2006). RAxML-VI-HPC: Maximum likelihood-based phylogenetic analyses with thousands of taxa and mixed models. Bioinformatics **22:** 2688–2690.

Südhof, T.C., and Rothman, J.E. (2009). Membrane fusion: Grappling with SNARE and SM proteins. Science **323:** 474–477.

Szymanski, D.B., and Cosgrove, D.J. (2009). Dynamic coordination of cytoskeletal and cell wall systems during plant cell morphogenesis. Curr. Biol. **19:** R800–R811.

Tominaga, M., Kojima, H., Yokota, E., Orii, H., Nakamori, R., Katayama, E., Anson, M., Shimmen, T., and Oiwa, K. (2003). Higher plant myosin XI moves processively on actin with 35 nm steps at high velocity. EMBO J. **22:** 1263–1272.

Tominaga, M., and Nakano, A. (2012). Plant-specific myosin XI, a molecular perspective. Front. Plant Sci. **3:** 211.

Ueda, H., Yokota, E., Kutsuna, N., Shimada, T., Tamura, K., Shimmen, T., Hasezawa, S., Dolja, V.V., and Hara-Nishimura, I. (2010). Myosin-dependent ER motility and F-actin organization in plant cells. Proc. Natl. Acad. Sci. USA **107:** 6894–6899.

Vale, R.D. (2003). The molecular motor toolbox for intracellular transport. Cell **112:** 467–480.

Vidali, L., Burkart, G.M., Augustine, R.C., Kerdavid, E., Tüzel, E., and Bezanilla, M. (2010). Myosin XI is essential for tip growth in *Physcomitrella patens*. Plant Cell **22:** 1868–1882.

Wang, G., Wang, F., Wang, G., Wang, F., Zhang, X., Zhong, M., Zhang, J., Lin, D., Tang, Y., Xu, Z., and Song, R. (2012). Opaque1 encodes a myosin XI motor protein that is required for endoplasmic reticulum motility and protein body formation in maize endosperm. Plant Cell **24:** 3447–3462.

Wang, Z., Edwards, J.G., Riley, N., Provance, D.W., Jr., Karcher, R., Li, X.D., Davison, I.G., Ikebe, M., Mercer, J.A., Kauer, J.A., and Ehlers, M.D. (2008). Myosin Vb mobilizes recycling endosomes and AMPA receptors for postsynaptic plasticity. Cell **135:** 535–548.

Woolfson, D.N., Bartlett, G.J., Bruning, M., and Thomson, A.R. (2012). New currency for old rope: From coiled-coil assemblies to α-helical barrels. Curr. Opin. Struct. Biol. **22:** 432–441.

Woolner, S., and Bement, W.M. (2009). Unconventional myosins acting unconventionally. Trends Cell Biol. **19:** 245–252.

Zhang, C., Kotchoni, S.O., Samuels, A.L., and Szymanski, D.B. (2010). SPIKE1 signals originate from and assemble specialized domains of the endoplasmic reticulum. Curr. Biol. **20:** 2144–2149.

Zhang, L., Zhang, H., Liu, P., Hao, H., Jin, J.B., and Lin, J. (2011). *Arabidopsis* R-SNARE proteins VAMP721 and VAMP722 are required for cell plate formation. PLoS ONE **6:** e26129.

Zheng, M., Beck, M., Müller, J., Chen, T., Wang, X., Wang, F., Wang, Q., Wang, Y., Baluska, F., Logan, D.C., Samaj, J., and Lin, J. (2009). Actin turnover is required for myosin-dependent mitochondrial movements in *Arabidopsis* root hairs. PLoS ONE **4:** e5961.